IEEE Access
Multidisciplinary ⋮ Rapid Review ⋮ Open Access Journal

Received September 29, 2021, accepted October 11, 2021, date of publication October 13, 2021, date of current version October 21, 2021.

Digital Object Identifier 10.1109/ACCESS.2021.3119782

Multi-Battery Block Module Power Converter for Electric Vehicle Driven by Switched Reluctance Motors

XIAOSHU ZAN[1,2], (Member, IEEE), GUANQUN XU[2], TIEJUN ZHAO[2], RUIMING WANG[1], AND LINWANG DAI[1]

[1]State Key Laboratory of Operation and Control of Renewable Energy and Storage Systems (China Electric Power Research Institute), Beijing 100000, China
[2]School of Electrical and Electronic Engineering, China University of Mining and Technology, Xuzhou 221116, China

Corresponding author: Guanqun Xu (ts20130201p31@cumt.edu.com)

This work was supported by the Open Fund of the State Key Laboratory of Operation and Control of Renewable Energy and Storage System (China Electric Power Research Institute) under Grant NYB51202001602.

ABSTRACT To improve the endurance and charging flexibility of electric vehicle battery packs, this paper proposes a multi-battery block module (MBM) topology for four-phase switched reluctance motors (SRMs), which not only allows flexible electric vehicle operation, but also achieves fast demagnetization and excitation. By integrating the multi-battery block module and photovoltaic (PV) panel into an asymmetrical half-bridge (AHB) converter, the MBM topology is designed to supply a multilevel bus voltage for the SRM drive. To improve the endurance of battery packs, a PV panel is also added to the topology to charge battery packs when the system is stationary. According to the different operation requirements, multiple power supply modes and charging modes can be realized by controlling the power devices in the proposed MBM topology. The simulation results based on the MATLAB/Simulink platform and the experimental results on a four-phase 8 / 6 switched reluctance motor verify the effectiveness of the proposed design.

INDEX TERMS Switched reluctance motors, electric vehicle, multi-battery block module, charge.

I. INTRODUCTION

Human survival is closely related to social progress and energy development. With the continuous progress of science and technology, people have to face new crises and challenges [1], [2], especially the contradiction that the energy demand is increasing, but the existing fossil energy is increasingly short [3], [4]. Developing new energy instead of fossil energy consumption to alleviate the energy crisis and reduce greenhouse gas emissions has become the main goal of global energy development in the future [5]–[7]. The development of new energy and related technologies has attracted increasing attention [8]–[10]. Making full use of renewable energy such as wind energy, solar energy and carrying out rational and effective energy management are important ways to deal with threats such as energy crises and environmental pollution [11], [12]. In the field of transportation, new energy electric vehicles that rely less on traditional fossil fuels have become an emerging way to alleviate the energy crisis because their low running cost and emissions [13], [14]. Simultaneously, with the development of smart grids and the popularity of charging piles, new energy electric vehicles have achieved rapid development and promotion [15], [16].

The SRM is a new type of motor. Its stator and rotor are both convex pole structures. The winding is not required by the rotor and a centralized winding is employed on the stator. The SRM power converter is the core of the SRM speed control system, and the design and selection of the power converter have a direct impact on the system performance [17]–[19]. Traditional power converters cannot meet the complex power supply needs of new energy electric vehicles. Additional circuitry is needed to charge the battery packs, which increases the system complexity [20], [21].

The multi-battery pack module in an electric vehicle is generally composed of multiple batteries and backup batteries, each of which has multiple single batteries. It is necessary to select different numbers of batteries that meet the operational requirements to participate in the power supply according to the operating conditions and the remaining capacity of the batteries. Therefore, it is important to design a power

The associate editor coordinating the review of this manuscript and approving it for publication was Moussa Boukhnifer.

converter which can flexibly combine multiple battery packs to meet the complex running conditions of electric vehicles. To meet the requirements of multi-battery charging flexibility and improving the endurance of electric vehicles, Scholars have further exploited the application of batteries in electric vehicles. Cascaded converters for SRM were studied in [22]–[24]. Reference [22] integrated a battery pack into an AHB converter to realize the flexible energy conversion between the generator, battery pack and motor, which can configure the multilevel bus voltage and current capacity, so as to accelerate the excitation and demagnetization in the commutation region. However, as the DC-link voltage reaches higher levels, the switching losses increase. The integrated power converter proposed in [23] connects the Buck converter with the AHB converter in series, which can accelerate the demagnetization process. However, it is only suitable for the buck charging mode in which the charging current is low. Hence, adapting the converter to both buck and boost charging modes becomes the target of this paper. The dual-front-end circuit with photovoltaic panel (PV) feed proposed in [24] does not need to be connected to the charging station for charging. It implements six driving modes and five charging modes, but an additional converter is required during charging.

The topology of the SRM drive is optimized and improved in [25]–[27] to meet the requirements of different working conditions. Reference [25] proposed an integrated battery-driven converter for the SRM, which can charge an on-board battery. In the driving mode, the SRM drive is powered by the booster, and a well-regulated DC connection voltage is established. During each demagnetization and continuation period, the energy stored in the winding is recharged to the battery. Reference [26] proposed a four-phase hysteresis-control SRM driver for driving electric vehicles. Hysteresis control is used for low-speed operations. This simple control can be used for electric vehicles specially designed for subways. A multifunctional SRM driver for single-phase and three-phase AC charging is introduced in [27]. Power converter topologies with a large number of power devices are relatively expensive and increase the difficulty of manufacturing [28]. To overcome these inherent drawbacks of complex topologies, several modular power converters have been proposed in [28]–[30]. Reference [28] proposed an SRM modular power converter based on dual-switch modules and dual-wire windings. However, it requires two-wire windings and is not suitable for the traditional SRM. In [29], a distributed SRM driver based on a modular multilevel converter for hybrid vehicle batteries is proposed. The battery pack is connected to the half-bridge converter as a sub-module and has multiple sub-modules connected, but the bus voltage is reduced and the excitation and demagnetization processes are prolonged. The modular power converter for a four-phase SRM proposed in [30] has the advantage of overlapping current pulses, which can increase the speed of the SRM and minimize the number of power switch modules. In addition, owing to the inherent working mechanism, this

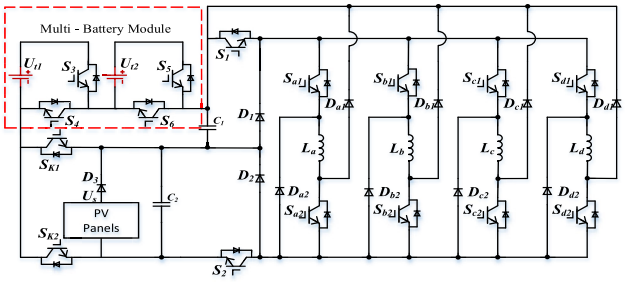

FIGURE 1. Multi-battery block module topology of the switched reluctance motor.

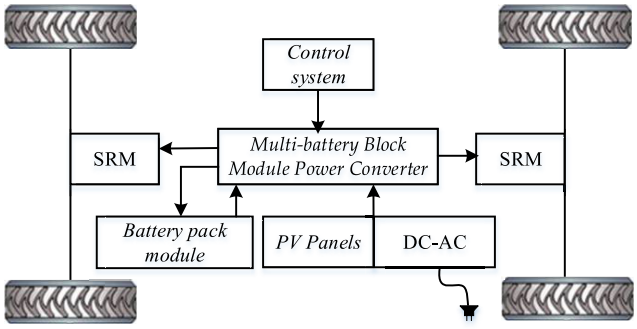

FIGURE 2. The electric vehicle drive system.

modular power converter improves the motor performance throughout the variation range of the motor characteristics.

In this paper, an MBM topology is proposed to realize a flexible combination of multiple batteries and adapt to the complex operation of electrical vehicles. The two battery packs and PV panels can achieve seven power supply modes by controlling power switches, thus improving the system flexibility. Three battery static charging methods can be realized, and the charging current can be flexibly adjusted which contributes to an improved battery life.

II. MULTI-BATTERY BLOCK MODULE POWER CONVERTER TOPOLOGY

A. SWITCHED RELUCTANCE MOTOR

Ignoring the iron loss and mutual inductance between phase windings, the electromechanical energy conversion of SRM system is analyzed. The N-phase voltage is as follows [31]:

$$\begin{aligned} \mathrm{U}_n &= R_n + \frac{d\psi_n}{dt} \\ &= R_n + \frac{\partial \psi_n}{\partial i_n}\frac{di_n}{dt} + \frac{\partial \psi_n}{\partial \theta_n}\frac{d\theta_n}{dt} \\ &= R_n + L_n(\theta_n, i_n)\frac{di_n}{dt} + \frac{\partial L_n(\theta_n, i_n)}{\partial \theta_n}\omega_r i_n \\ &= R_n + L_n(\theta_n, i_n)\frac{di_n}{d\theta_n}\omega_r + \frac{\partial L_n(\theta_n, i_n)}{\partial \theta_n}\omega_r i_n \end{aligned} \quad (1)$$

where U_n is the phase N supply voltage, R_n is the phase N resistance, in is the phase N current, L_n is the phase N inductance, Ψ_n is the phase N magnetic flux, and θ_n is the rotor position angle, ω_r is the rotor angular velocity.

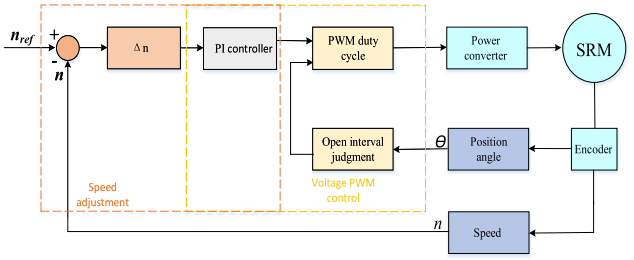

FIGURE 3. Control block diagram of SRM.

B. TOPOLOGY AND OPERATION MODE ANALYSIS

To better meet the operational requirements of battery power supply and charging in electric vehicles, a MBM power converter is designed as shown in Figure 1. The power converter is composed of a multi-battery module, chopper charging circuit and dual-bus asymmetric half-bridge circuit. The multi-battery pack module consists of two battery packs.

An electric vehicle driven by an SRM, which has multiple driving and charging modes is shown in Figure 2.

Figure 3 presents the block diagram of the control strategy of the SRM system where a PWM control method is employed. The PWM control system has excellent control accuracy, in which the excitation voltage and phase current can be easily regulated by changing the duty cycle of PWM wave. The control precision is high and the effect is good. The switching signals are derived from the comparison of the motor speed reference and actual speed. The rotor position is detected by an encoder for speed calculation, and the turn-on and turn-off angles are calculated for phase commutation. To realize closed-loop control, a proportional integral (PI) controller is also employed to regulate the motor speed.

Figure 4(a) shows the normal power supply mode in which switch S_{K1} is on and S_{K2} is off. By controlling switches S_3 and S_5, the MBM converter can perform three different modes of power supply, namely, the battery pack BP_1 participating in power supply alone, the battery pack BP_2 participating in power supply alone and the battery pack BP_1 and the battery pack BP_2 participating in power supply together. Four methods of power supply in which PV panels participate can be implemented: the power supply with PV panels alone, the power supply with PV panels and battery pack BP_1 together, power supply with PV panels and battery pack BP_2 together and power supply with photovoltaic panels and battery packs BP_1 and BP_2 together. By controlling S_4 and S_6, three freewheeling modes can be achieved: freewheeling current passes through battery BP_1 and battery BP_2 (freewheeling mode 1), freewheeling current only passes through battery BP_1 (freewheeling mode 2), freewheeling current only passes through battery BP_2 (freewheeling mode 3). Through different combinations, a total of 13 freewheeling charging modes can be realized under seven power supply situations.

Figure 4 (a) shows the path of the phase A current in the excitation stage when battery pack BP_1 supplies power alone. Under this condition, switch S_3 is on and switch S_5 is off, and the power supply current only flows through BP_1.

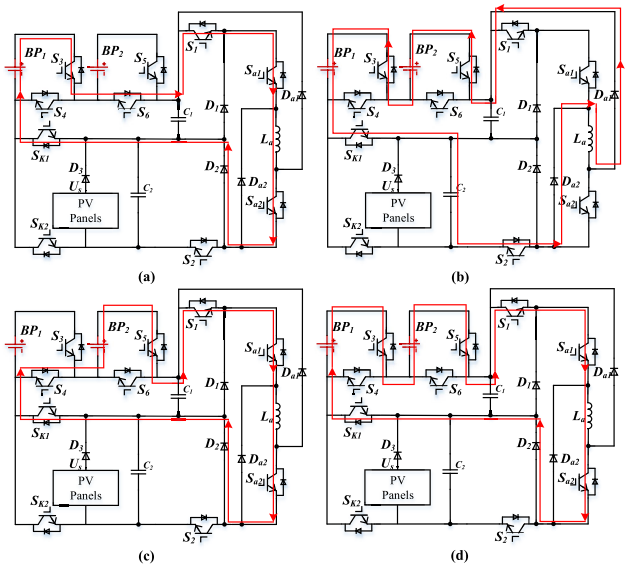

FIGURE 4. Operation mode of MBM converter (a) powered by battery packs BP_1. (b) freewheeling mode 1. (c) powered by battery packs BP_2. (d) powered by battery packs BP_1 and BP_2.

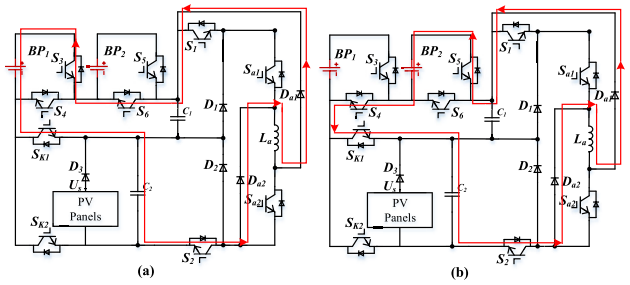

FIGURE 5. Freewheeling operation mode. (a) freewheeling mode 2. (b) freewheeling mode 3.

Figure 4(c) shows the path of the phase A current in the excitation stage when battery pack BP_2 participates in the power supply separately. Under this condition, switch S_5 is on, switch S_3 is off, and the power supply current passes through battery pack BP_2 only. Figure 4 (d) shows the circuit diagram of phase A current in the excitation stage when the battery packs BP_1 and BP_2 are both involved in the power supply. Under this condition, switches S_3 and S_5 are all on, and the power supply current passes through battery packs BP_1 and BP_2.

By comparing the three combination forms of the battery pack, it can be found that the battery packs that participate in the power supply can be adjusted by simply controlling switches S_3 and S_5 to adapt to various operation states of new energy electric vehicles.

Because the on-off conditions of switches S_3, S_4, S_5, S_6 are different under the seven power supply modes, the freewheeling modes that can be realized under the seven power supply modes are also different. When the battery pack BP_1 participates in the power supply separately, switch S_3 is on and switches S_4, S_5 are off, two freewheeling modes can be realized. When switch S6 is off, the SRM can realize

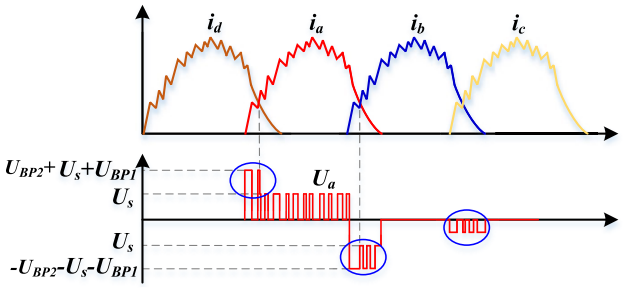

FIGURE 6. Phase A voltage waveform of SRM powered by PV panel.

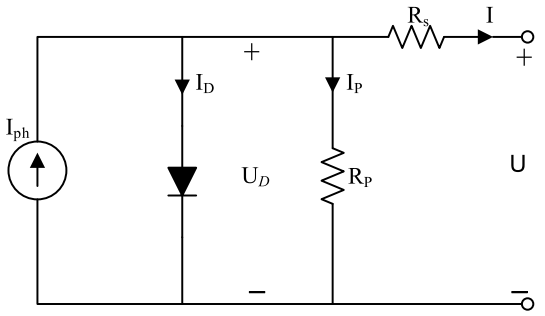

FIGURE 7. The simple diode model of a PV cell.

the freewheeling mode1. The circuit diagram of the phase A current in the freewheeling stage in this mode is shown in Figure 4 (b), where the freewheeling current flows through the battery pack BP_1 and the battery pack BP_2. Similarly, when switch S_6 is on, freewheeling mode2 can be realized. Figure 5 (a) shows that the freewheeling current of phase A only flows through the battery BP_1 to charge it.

When the battery pack BP_2 is independently involved in the power supply, switch S_5 is on and S_3 is off. Similarly, switch S_6 must be turned off under the influence of switch S_5. The SRM can also realize two freewheeling modes. When switch S4 is off, the freewheeling mode 2 shown in Figure 5 (a) can be realized, whereas when switch S_4 is on, the freewheeling mode 2 shown in Figure 5 (b) can be realized. The freewheeling current of phase A only flows through battery pack BP_2. When battery packs BP_1 and BP_2 participate in the power supply together, switches S_3 and S_5 are turned on, and switches S_4 and S_6 are kept shut down. Under this condition, only freewheeling mode 1, as shown in Figure 4 (b) can be realized.

By controlling switches S_3 and S_5, three power supply modes of battery packs can be realized. Combined with the control of switches S_1 and S_2, a total of seven power supply modes can be implemented, including three separate power supply modes of battery packs, three hybrid power supply modes of photovoltaic panels and battery packs and the power supply of photovoltaic panels. Three types of current-continuum charging can be realized by controlling switches S_4 and S_6. However, considering that the conduction of switches S_3 and S_5 will affect switches S_4 and S_6, three freewheeling modes can be all realized only when PV panels supplies power alone. Only a part of the freewheeling mode can be realized under the other power supply modes. The combination of various power supply modes and continuous current charging forms makes the utilization of the battery pack more reasonable, and a variety of flexible control methods improve the reliability of the system.

C. OPERATION MODE ANALYSIS OF SRM

Figure 6 shows the waveforms of phase A under the mode that battery pack BP_1 supplies power alone under freewheeling mode 1 where S_6 is off to analyze operation mode of SRM. When phase A enters the excitation stage and the current i_d of phase D is greater than that of phase A, the current i_d of phase D will not only flow through the battery pack BP_1 and the energy storage capacitance C_2, but also through phase A to form the excitation current for fast excitation, where the voltage of phase D and phase A are

$$U_d = -U_{BP1} - U_{BP2} - U_s \tag{2}$$

$$\begin{aligned} U_a &= -U_d \\ &= U_{BP1} + U_{BP2} + U_s \\ &= i_a R_a + L_a \omega_r \frac{di_a}{d\theta_a} + i_a \omega_r \frac{dL_a}{d\theta_a} \end{aligned} \tag{3}$$

where U_d is the voltage of phase D, U_a is the voltage of phase A, U_{BP1} and U_{BP2} is battery pack voltage, U_s is the PV panel voltage, L_a is the phase A inductance, i_a is the phase A current, θ_a is the rotor position angle of phase A, and ω_r is the rotor angular velocity.

When phase A enters the demagnetization stage and phase B is not on yet or the excitation current i_b of phase B is less than the freewheeling current i_a of phase A, the freewheeling current of phase A flows back to the capacitance and the battery pack BP_1. When phase A is subjected to a high reverse voltage, fast demagnetization can be achieved, where the voltage of phase A is:

$$U_a = -U_{\mathrm{BP1}} - U_{BP2} - U_s \tag{4}$$

When phase A is off and phases B or C is in the demagnetizing stage, the phase A winding generates a small inductive current because the demagnetizing voltage is a pulse alternating voltage, not a single-level demagnetizing voltage driven by a traditional asymmetric half-bridge topology circuit. In this case, the winding voltage of phase A is:

$$U_a = -L_a \frac{di_a}{dt} \tag{5}$$

When the battery pack BP_1 and BP_2 supply power together and the battery BP_2 participates in the power supply alone, the operation process of the system is similar to that of the battery pack BP_1 supply power separately, but the excitation and demagnetization voltage levels of different modes are different.

D. MODEL OF PHOTOVOLTAIC PANEL

As is shown in figure 7, the paper uses a single diode model consisting of diodes and resistors for analysis. The power

source coupled in parallel with a semiconductor diode shapes an ideal cell, plus the two electrical resistors R_S, R_P that shape the current and voltage losses [32]

The voltage-current characteristic of a diode is expressed according to the relationship below

$$I_D = I_s \cdot [e^{\frac{e}{KT}U_D} - 1] \tag{6}$$

where I_D is the current of diode, U_D is the diode voltage, I_s is the reverse saturation current, T is the thermodynamic temperature, K is the Boltzmann constant.

The current produced by the source I_{ph} depends on the intensity of the solar radiation, the absorption coefficient of the wavelength of the solar radiation, and the diffusion and electron recombination characteristics of the material according to the relationship below

$$I_{ph} = -I_{ph,STC} \cdot \frac{G}{G_{STC}} \cdot [1 + \alpha_1 \left(T_c - T_{c,STC}\right)] \tag{7}$$

where G is the solar radiation measured, G_{STC} - the solar radiation in standard conditions (1000W/m^2), $T_{c,STC}$ -temperature at STC (298.15 K).

By applying the Kirchhoff theorem to the circuit in Fig. 8, the voltage-current characteristic of a photovoltaic cell is obtained as follows

$$I = \frac{U + I_D R_s}{R_p} \tag{8}$$

By substituting Id and Ip with their expressions we obtain:

$$I = I_{ph} - I_S(e^{\frac{q(U+I\cdot R_S)}{\alpha K T_c}} - 1) - \frac{U + I_D R_s}{R_p} \tag{9}$$

where I is the current of PV cell, U is the voltage of PV cell, I_D is the current of diode, α is a constant related to the PV junction (Usually between 0 and 1)

E. STATIC CONTINUOUS CHARGING MODE

When the SRM is still, the battery is no longer involved in the power supply, switches S_1, S_3, and S_5 are off, and the system can realize three types of charging modes. Taking the battery pack BP_2 supplying power separately as an example, when the switch S_{K1} is off and S_{K2} is on, the system changes from the power supply operation mode to the charging operation mode. In order to maintain the static operation, the switch tubes on the other three-phase bridge arms of B, C, and D are kept shut off, and switches S_{K2}, S_{a1} and S_{a2} are controlled to enter the static continuous charging mode. As shown in Figure 8 (a), when switches S_{a1}, S_{a2} are on and S_{K2} is off, the PV panels charge for phase A winding. As shown in Figure 8 (b), when switch S_{K2} is on and S_{a1}, S_{a2} are off, phase A winding is charged by the battery pack BP_2. The charge current can be easily regulated by controlling the PWM duty cycle and frequency of S_{K2}, S_{a1}, and S_{a2}. The phase A winding current i_a is:

$$i_a(t) = i_{a0} + \frac{(i_{am} - i_{a0})t}{T} D \tag{10}$$

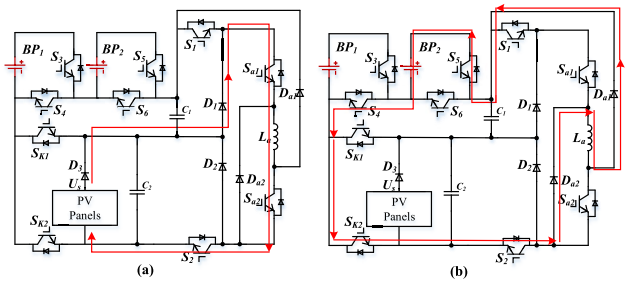

FIGURE 8. Static freewheeling charging mode. (a) stage 1 (b) stage 2.

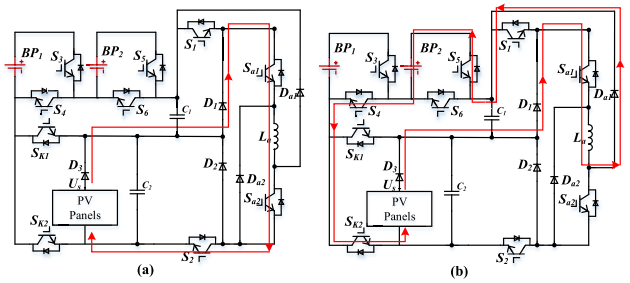

FIGURE 9. Boost charging mode of MBM converter. (a) stage 1 (b) stage 2.

The battery charge current i_c is:

$$i_c(t) = i_{a0} - \frac{i_{am} - i_{a0}}{(1-D)T}(t - DT) \tag{11}$$

i_{a0} and i_{am} are the initial phase current and the maximum phase current of phase A, respectively; D is the duty cycle of switches S_{a1} and S_{a2}, and T is the switching period.

F. BOOST CHARGING MODE

Similarly, the battery pack BP_2 supplying power separately is taken as an example for analysis. After closing switch S_{K1}, system enters the charging operation mode of the battery pack, switch S_{K2} and S_{a2} are controlled to enter the boost charging mode. As shown in Figure 9 (a), when switches S_2, S_{a1} and S_{a2} are turned on and S_{K2} is turned off, the PV panels charge phase A winding while battery pack BP_2 is charged by capacitor C_1. As shown in Figure 9 (b), when switches S_{a1}, and S_{K2} are on and S_2, and S_{a2} are off, the PV panels and phase A winding are charged by the BP_2 battery pack at the same time. The charging current can be easily regulated by controlling the PWM duty cycle and the frequencies of S_{K2} and S_{a2}.

G. BUCK CHARGING MODE

The battery pack BP_2 supplying power alone is still considered as an example. Switches S_{K1} and S_{a2} are off, and switch S_{K2} is on. At this time, the system enters the charging operation mode of the battery pack, and enters the buck charging mode by controlling switch S_{a1}. As shown in Figure 10 (a), when switch S_{a1} is on, the PV panel charges the phase A winding and battery BP_2. As shown in Figure 10 (b), when the S_{a1} is off, the battery pack BP_2 is charged by the phase

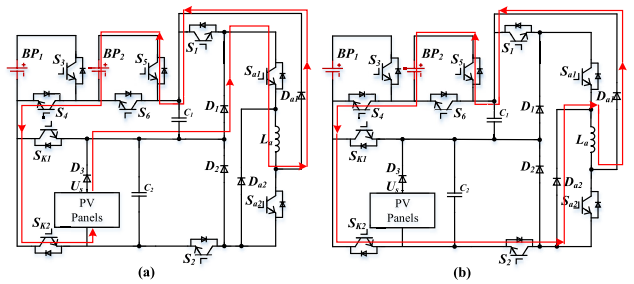

FIGURE 10. Buck charging mode of MBM converter. (a) stage 1 (b) stage 2.

TABLE 1. Simulation parameters.

system parameter	value
Phase number	4
Rotor pole number	6
Stator pole number	8
Rated power	500V
Opening angle	5°
Turn-off angle	20°
Battery pack BP_1 volage	36V
Battery pack BP_2 volage	24V
PV panels voltage	30V
PV panels rated power	200W

A winding. The charging current can be easily regulated by controlling the PWM duty cycle and frequency of S_{a1} and S_2.

III. SIMULATION

In this section, the simulation model of a four-phase 8/6 SRM system driven by an MBM power converter is built in MATLAB / Simulink and an operation analysis is carried out. The parameters of the model are listed in Table 1

The perturbation observation method is employed in PV panels to guarantee a voltage of 30V at the maximum power point.

Figure 11 shows simulation waveforms of freewheeling mode 1 and 2 when the battery pack BP_1 participates in the power supply alone, the switch S_3 is on and switches S_4, S_5 are off, by controlling switch S_6, two freewheeling modes can be realized. The simulation waveform of the freewheeling mode 1 when the switch S_6 is off is shown in Figure 11 (a). The excitation voltage of phase A is 90 V which is the sum of the voltage of the two battery packs and the photovoltaic panel, and the demagnetization voltage is −36 V and −90 V. The freewheeling current flows through the battery pack BP_1 and the battery pack BP_2 to charge the two battery packs. When the switch S_6 is on, freewheeling mode 2 can be realized. The simulation waveform of the freewheeling mode 2 is shown in figure 11 (b). It can be seen that the

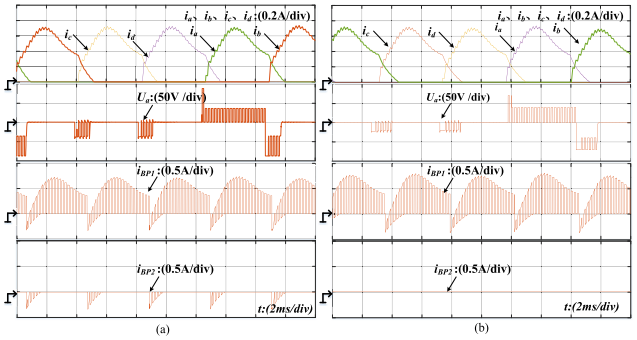

FIGURE 11. Simulation operation waveforms of SRM supplied separately by battery block BP_1. (a) freewheeling mode 1. (b) freewheeling mode 2.

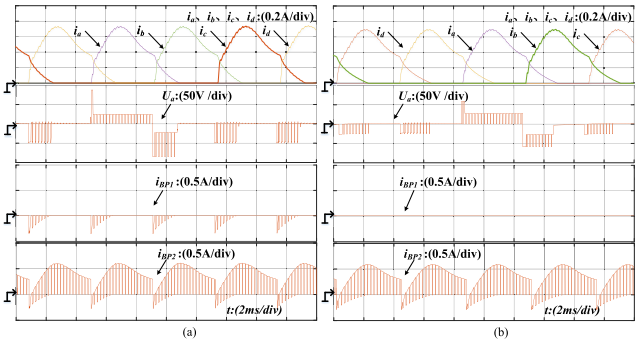

FIGURE 12. Simulation operation waveforms of SRM supplied separately by battery block BP_2. (a) freewheeling mode 1. (b) freewheeling mode 2.

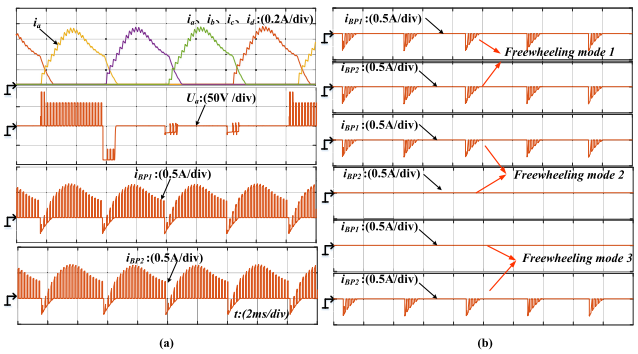

FIGURE 13. Simulation operation waveforms of MBM converter. (a) powered by battery packs BP_1 and BP_2 (b) powered by PV panels.

excitation voltage of phase A is 66 V, the demagnetization voltage is −36 V and −66 V, the freewheeling current only flows through the battery BP_1 for its charging.

Figure 12 shows simulation waveforms of freewheeling mode 1 and 2 when the battery pack BP_2 participates in the power supply alone, the switch S_5 is on and switches S_3, S_6 are off, by controlling switch S_4, two freewheeling modes can be realized. The simulation waveform of the freewheeling mode 1 when the switch S_4 is off is shown in Figure 12 (a). The excitation voltage of phase A is 90 V which is the sum of the voltage of the two battery packs and the photovoltaic panel, and the demagnetization voltage is −24 V and −90 V. The freewheeling current flows through the battery pack BP_1 and the battery pack BP_2. When the

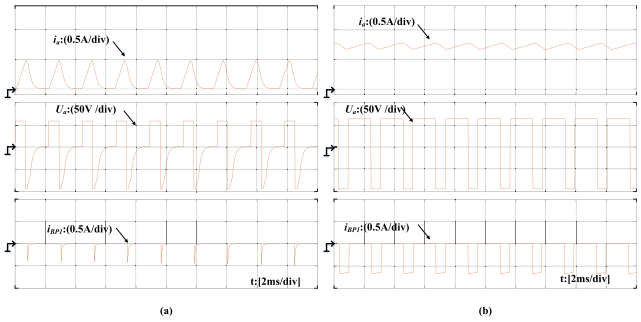

FIGURE 14. Simulation operation waveforms of static freewheeling charging mode. (a) At 30% duty cycle. (b) At 70% duty cycle.

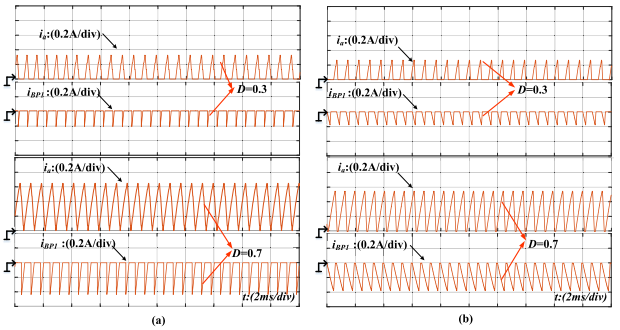

FIGURE 15. Simulation operation waveforms of chopping charging mode. (a) Boost charging mode. (b) Buck charging mode.

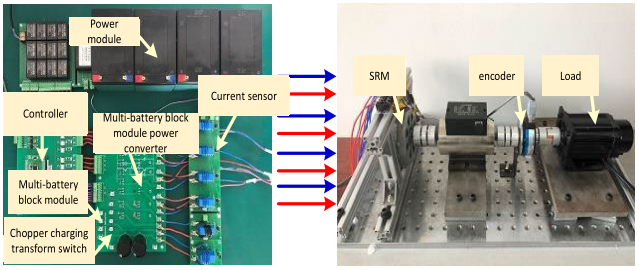

FIGURE 16. Experimental platform.

switch S_4 is on, freewheeling mode 2 can be realized. The simulation waveform of the freewheeling mode 2 is shown in figure 12 (b). It can be seen that the excitation voltage of phase A is 54 V which is the sum of the voltage of PV panel and the battery pack BP_2, the demagnetization voltage is −24 V and −54 V, the freewheeling current only flows through the battery BP_2 for its charging.

The simulation waveform diagram of the SRM powered by batteries BP_1 and BP_2 together and separately by PV panels is shown in Figure 13. When the battery packs BP_1 and BP_2 participate in the power supply, switches S_3 and S_5 are on, and switches S_4 and S_6 are off. As shown in Figure 13 (a), there is only one freewheeling mode at this time, that is, the charging current flows through the battery pack BP_1 and the battery pack BP_2 to charge the two battery packs.

When powered by PV panels alone, switches S_3 and S_5 are off, and switches S_4 and S_6 are no longer affected by switches S_3 and S_5. As shown in Figure 13(b), three freewheeling modes can be all realized. In freewheeling mode 1, switches S_4 and S_6 are off, and the freewheeling current flows through battery BP_1 and the battery BP_2 to charge both of them. In freewheeling mode 2, switch S_4 is off and S_6 is on, and the freewheeling current only flows through battery BP_1. In freewheeling mode 3, switch S_4 is on and S_6 is off, and the freewheeling current only flows through battery BP_2.

Figure 14 shows the simulation waveforms of the static freewheeling charging mode. At this time, switches S_1, S_3, S_4 and S_5 are off and switch S_6 is on. The PV panels charge only the battery pack BP_1. Figure 14 (a) shows the simulation waveform when PWM duty cycle D of switches S_{a1} and S_{a2} is 0.3. Figure 14 (b) shows the simulation waveform when the PWM duty cycle D of switches S_{a1} and S_{a2} is 0.7. The simulation results show that with an increase in the duty cycle, the charging current increases and the charging current becomes more stable.

Taking the battery BP_1 supplying power alone as an example, the simulation waveforms of the buck and boost freewheeling charging modes are shown in Figure 15. Figure 15 (a) shows the simulation waveforms of the boost charging mode. The charging current can be effectively controlled by controlling the PWM duty cycle of switches S_{K2} and S_{a2}. By comparison, it can be observed that the current variation is the same as that in the static freewheeling charging mode. The charging current increased and became more stable with an increase in the duty cycle. Figure 15 (b) shows the waveforms for the buck charging mode. The charging current can be effectively controlled by controlling the PWM duty cycle of switch S_{a1}. The charging current also increases with an increase in duty cycle. By comparison, it can be found that the boost charging mode only charges the battery in the winding freewheeling stage, while the buck charging mode charges the battery during the entire process of winding charging and discharging. The charging effect was obvious, but the charging current decreased.

IV. EXPERIMENT

To verify the feasibility of the proposed MBM topology, experiments were carried out on a 500 W SRM converter with the same parameters. The experimental platform is illustrated in Figure 16. The switches of the new converter adopt internal fast recovery anti-parallel diode IGBT. The adjustable 30V DC power supply was used to simulate the PV panel power supply, and a 24V battery pack and a 36V battery pack were formed by 12V batteries in series. The rotor position is determined by a 1000line incremental encoder. The main control system is realized by a TMS320F28335 digital signal processor produced by Texas Instruments Company. The phase-current waveform was collected by a Hall effect current sensor.

Figure 17 shows the experimental waveforms of the A-phase winding current i_a, voltage U_a, and battery pack current i_{t1} and i_{t2} when SRM is only powered by battery BP_1. Figure 17 (a) shows the simulation waveforms of freewheeling mode 1. Figure 17 (b) shows the simulation waveform of

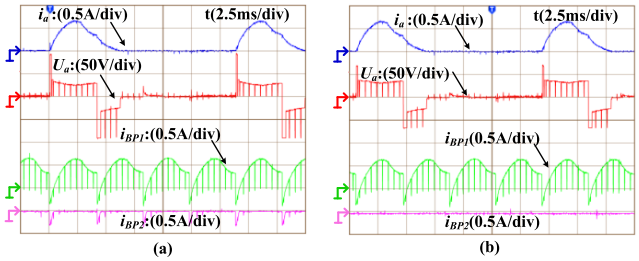

FIGURE 17. Experiment waveforms of multi-battery block module power converter. (a) freewheeling mode 1. (b) freewheeling mode 2.

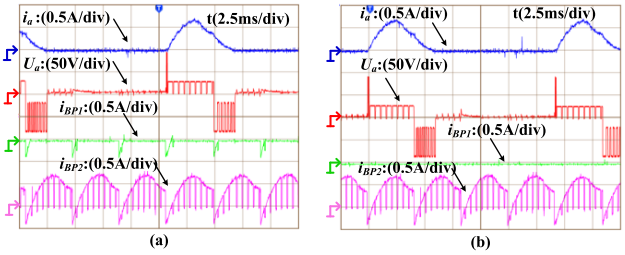

FIGURE 18. Experimental waveforms of SRM supplied separately by battery block BP_2. (a) freewheeling mode1 (b) freewheeling mode 2.

the freewheeling mode 2 of the SRM system when switch S_6 is on. It can be seen that SRM can realize high-level excitation and demagnetization in both freewheeling modes, which speeds up the excitation and demagnetization processes and improves the performance of the SRM system.

The experimental waveforms of the A-phase winding current ia, A-phase winding voltage U_a, BP_1 current i_{t1} and BP_2 current i_{t2} when the SRM is only powered by battery BP_2 is shown in Figure 18. Figure 18 (a) shows the simulation waveform of freewheeling mode 1, in which switch S_4 is off. The simulation waveform diagram of freewheeling mode 2 is shown in Figure 18 (b). Similar to the operation mode in which battery BP_1, supplies power alone, two freewheeling charging modes can also be realized when only powered by battery BP_2, but the A-phase voltage is different from the charging target, which fully improves the flexibility of the battery charging mode.

Figure 19 (a) shows the freewheeling mode when battery packs BP_1 and BP_2 supply power together, that is, the freewheeling current flows through battery BP_1 and battery BP_2 to charge both of them. Three freewheeling modes can be realized when only the PV panel is used for the power supply alone. As shown in Figure 19 (b), in freewheeling mode 1, switches S_4 and S_6 are off, and the freewheeling current flows through battery BP_1 and the battery BP_2 to charge both of them. In freewheeling mode 2, switch S_4 is off and S_6 is on, and the freewheeling current only flows through battery BP_1. In freewheeling mode 3, switch S_4 is on and S_6 is off, and the freewheeling current only flows through battery BP_2. By controlling a variety of freewheeling modes, the battery can be charged through the PV panel during the operation process, which fully improves the utilization rate of electric energy and the endurance of the vehicle.

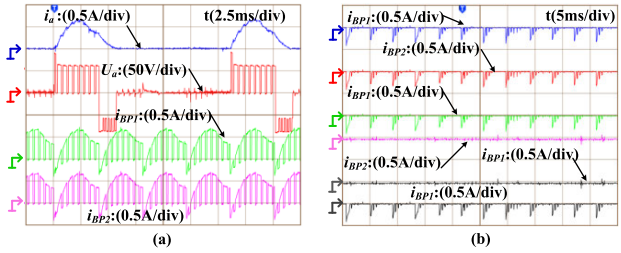

FIGURE 19. Experimental waveforms of multi-battery block module power converter. (a) powered by battery packs BP_1 and BP_2. (b) powered by PV panels.

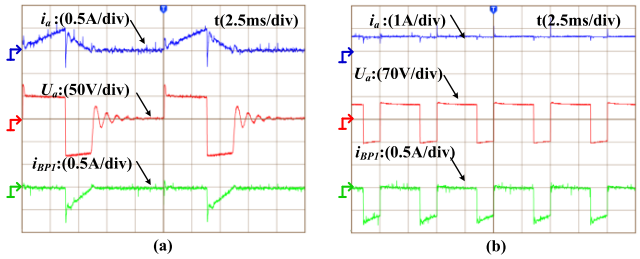

FIGURE 20. Experimental operation waveforms of static freewheeling charging mode. (a) At 30% duty cycle. (b) At 70% duty cycle.

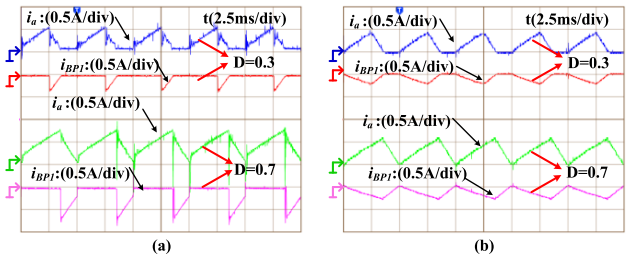

FIGURE 21. Experimental operation waveforms of chopping charging mode (a) Boost charging mode (b) Buck charging mode.

In Figure 20, the experimental waveforms under the static freewheeling charging mode are shown. Figure 20 (a) shows the experimental waveforms when the PWM duty cycle D of switches S_{a1} and S_{a2} is 0.3, and Figure 20(b) shows the experimental waveforms when the PWM duty cycle D of switches S_{a1} and S_{a2} is 0.7. It can be observed that the charging current increases with an increase in the duty cycle, which can better charge the battery pack.

The experimental waveforms of the phase A winding current i_a and battery pack BP_1 current i_{t1} under the chopping continuous current charging mode are shown in Figure 21. Figure 21 (a) shows the experimental waveforms of the booster charging mode. Through comparison, it can be found that the law of current variation is the same as that in the static continuous current charging mode. The charging current increases with an increase in the duty cycle of switches S_{K2} and S_{a2}, and the charging current is more stable. Figure 21 (b) shows the experimental waveforms of the buck-charging mode, where the charging current increases with an increase in the duty cycle of switch S_{a1}. By comparing the experimental waveforms, it can be found that the boost charging mode only charges the battery pack in the phase

winding current freewheeling stage, while the buck charging mode can charge the battery pack throughout the entire process. The buck charging mode has a better charging effect and the charging current increases significantly before switch S_{a1} is turned off. However, the charging current of the buck charging mode decreases.

V. CONCLUSION

Aiming at the complex operation requirements of electric vehicles, a multi-battery block module power converter topology is discussed and implemented. The advantages of the proposed topology are that by controlling the power switches in the battery module, multiple combinations of power supply and freewheeling charging of multiple batteries during operation can be achieved and adapted to the complex and changeable operation requirements. It can realize three different static charging methods: static freewheeling charging, boost charging and buck charging. The charging current can be adjusted flexibly. A variety of charging methods can better adapt to the charging requirements of different batteries and improve the service life of batteries. In the battery module, a small number of switches can be used to charge different batteries flexibly, which improves the power utilization efficiency and endurance.

REFERENCES

[1] J. Lu, Y. Hu, G. Chen, Z. Wang, and J. Liu, "Mutual calibration of multiple current sensors with accuracy uncertainties in IPMSM drives for electric vehicles," *IEEE Trans. Ind. Electron.*, vol. 67, no. 1, pp. 69–79, Jan. 2020.

[2] C. Gong, Y. Hu, J. Gao, Y. Wang, and L. Yan, "An improved delay-suppressed sliding-mode observer for sensorless vector-controlled PMSM," *IEEE Trans. Ind. Electron.*, vol. 67, no. 7, pp. 5913–5923, Jul. 2020.

[3] C. Gong, Y. Hu, and C. Gan, "Modeling, analysis, and attenuation of uncontrolled generation for IPMSM-based electric vehicles in emergency," *IEEE Trans. Ind. Electron.*, vol. 67, no. 6, pp. 4453–4462, Jun. 2020.

[4] X. Zan, K. Ni, W. Zhang, Z. Jiang, M. Cui, D. Yu, and R. Zeng, "A new control strategy for SR generation system based on modified PT control," *IEEE Access*, vol. 7, pp. 179720–179733, 2019.

[5] Y. Liu, G. Chen, Y. Hu, L. Huang, and X. Qing, "Magnetic coupling branch based dual-input/output DC–DC converters with improved cross-regulation and soft-switching operation," *IEEE Trans. Ind. Electron.*, vol. 67, no. 9, pp. 7167–7178, Sep. 2020.

[6] J. Yang, D. Yu, H. Cheng, X. Zan, and H. Wen, "Dual-coupled inductors-based high step-up DC/DC converter without input electrolytic capacitor for PV application," *IET Power Electron.*, vol. 10, no. 6, pp. 646–656, May 2017.

[7] D. Yu, K. Li, S. Yu, H. Trinh, P. Zhang, A. M. T. Oo, and Y. Hu, "A novel power and signal composite modulation approach to powerline data communication for SRM in distributed power grids," *IEEE Trans. Power Electron.*, vol. 36, no. 9, pp. 10436–10446, Sep. 2021.

[8] Wang, R. Yang, and Y. Yu, "Sensorless control of interior permanent magnet synchronous motor," in *Proc. CSEE*, 2010, pp. 93–98.

[9] S. Song, G. Fang, R. Hei, J. Jiang, R. Ma, and W. Liu, "Torque ripple and efficiency online optimization of switched reluctance machine based on torque per ampere characteristics," *IEEE Trans. Power Electron.*, vol. 35, no. 9, pp. 9608–9616, Sep. 2020.

[10] L. Ge, I. Ralev, A. Klein-Hessling, S. Song, and R. W. De Doncker, "A simple reluctance calibration strategy to obtain the flux-linkage characteristics of switched reluctance machines," *IEEE Trans. Power Electron.*, vol. 35, no. 3, pp. 2787–2798, Mar. 2020.

[11] K. Ni, Y. Liu, Z. Mei, T. Wu, Y. Hu, H. Wen, and Y. Wang, "Electrical and electronic technologies in more-electric aircraft: A review," *IEEE Access*, vol. 7, pp. 76145–76166, 2019.

[12] C. Gan, Y. Chen, Q. Sun, J. Si, J. Wu, and Y. Hu, "A position sensorless torque control strategy for switched reluctance machines with fewer current sensors," *IEEE/ASME Trans. Mechatronics*, vol. 26, no. 2, pp. 1118–1128, Apr. 2021.

[13] C. Gong, Y. Hu, H. Wen, G. Chen, W. Li, and J. Gao, "Reliable winding-based DC-bus capacitor discharge technique over full-speed range for IPMSM drive in electric vehicles without position sensor," *IEEE Trans. Ind. Electron.*, vol. 67, no. 10, pp. 8131–8142, Oct. 2020.

[14] G. Chen, Z. Jin, Y. Liu, Y. Hu, J. Zhang, and X. Qing, "Programmable topology derivation and analysis of integrated three-port DC–DC converters with reduced switches for low-cost applications," *IEEE Trans. Ind. Electron.*, vol. 66, no. 9, pp. 6649–6660, Sep. 2019.

[15] C. Gong, Y. Hu, G. Chen, H. Wen, Z. Wang, and K. Ni, "A DC-bus capacitor discharge strategy for PMSM drive system with large inertia and small system safe current in EVs," *IEEE Trans. Ind. Informat.*, vol. 15, no. 8, pp. 4709–4718, Aug. 2019.

[16] C. Gong, Y. Hu, W. Li, J. Gao, J. Liu, H. Wen, and J. Yang, "Hybrid DC-bus capacitor discharge strategy using internal windings and external bleeder for surface-mounted PMSM-based EV powertrains in emergency," *IEEE Trans. Ind. Electron.*, vol. 68, no. 3, pp. 1905–1915, Mar. 2021.

[17] C.-Y. Lim, Y. Jeong, M.-S. Lee, K.-H. Yi, and G.-W. Moon, "Half-bridge integrated phase-shifted full-bridge converter with high efficiency using center-tapped clamp circuit for battery charging systems in electric vehicles," *IEEE Trans. Power Electron.*, vol. 35, no. 5, pp. 4934–4945, May 2020.

[18] D. Yu, Y. Hua, S. Yu, P. Zhang, H. H. C. Iu, and T. Fernando, "A new modulation–demodulation approach to DC power-line data transmission for SRG-integrated microgrid," *IEEE Trans. Power Electron.*, vol. 35, no. 11, pp. 12370–12382, Nov. 2020.

[19] S. Song, R. Hei, R. Ma, and W. Liu, "Model predictive control of switched reluctance starter/generator with torque sharing and compensation," *IEEE Trans. Transport. Electrific.*, vol. 6, no. 4, pp. 1519–1527, Dec. 2020.

[20] X. Zan, Z. Jiang, K. Ni, W. Zhang, Y. Gong, and N. Wu, "Modular battery management for SRM drives in hybrid vehicles based on a novel modular converter," *IEEE Access*, vol. 8, pp. 136296–136306, 2020.

[21] Z. Yu, C. Gan, K. Ni, Y. Chen, and R. Qu, "Dual-electric-port bidirectional flux-modulated switched reluctance machine drive with multiple charging functions for electric vehicle applications," *IEEE Trans. Power Electron.*, vol. 36, no. 5, pp. 5818–5831, May 2021.

[22] Q. Sun, J. Wu, C. Gan, J. Si, J. Guo, and Y. Hu, "Cascaded multiport converter for SRM-based hybrid electrical vehicle applications," *IEEE Trans. Power Electron.*, vol. 34, no. 12, pp. 11940–11951, Dec. 2019.

[23] J. Cai and X. Zhao, "An on-board charger integrated power converter for EV switched reluctance motor drives," *IEEE Trans. Ind. Electron.*, vol. 68, no. 5, pp. 3683–3692, May 2021.

[24] C. Gan, N. Jin, Q. Sun, W. Kong, Y. Hu, and L. M. Tolbert, "Multiport bidirectional SRM drives for solar-assisted hybrid electric bus powertrain with flexible driving and self-charging functions," *IEEE Trans. Power Electron.*, vol. 33, no. 10, pp. 8231–8245, Oct. 2018.

[25] D. Gao, Z. Jin, J. Zhang, J. Li, and M. Ouyang, "Development and performance analysis of a hybrid fuel cell/battery bus with an axle integrated electric motor drive system," *Int. J. Hydrogen Energy*, vol. 41, no. 2, pp. 1161–1169, Jan. 2016.

[26] A. George, K. P. Pinkymol, and J. Cherian, "Battery powered 4-phase 8/6 pole SRM drive for advanced electric vehicle," *Innov. Power Adv. Comput. Technol.*, Vellore, India, Apr. 2017, pp. 1–8.

[27] N. Sakr, A. Fernandez Sanchez, D. Sadarnac, and A. Gascher, "A combined switched reluctance motor drive and battery charger for electric vehicles," in *Proc. 41st Annu. Conf. IEEE Ind. Electron. Soc.*, Yokohama, Japan, Nov. 2015, pp. 1770–1775.

[28] X. D. Xue, K. W. E. Cheng, and Y. J. Bao, "Control and integrated half bridge to winding circuit development for switched reluctance motors," *IEEE Trans. Ind. Informat.*, vol. 10, no. 1, pp. 109–116, Feb. 2014.

[29] M. ElMenshawy and A. Massoud, "Development of modular DC-DC converters for low-speed electric vehicles fast chargers," *Alexandria Eng. J.*, vol. 60, no. 1, pp. 1067–1083, Feb. 2021.

[30] D. S. Mihic, M. V. Terzic, B. M. Brkovic, and S. N. Vukosavic, "A novel modular power converter for SRM drive," *Electr. Eng.*, vol. 102, no. 2, pp. 921–937, Jun. 2020.

[31] X. Zan, W. Zhang, K. Ni, Z. Jiang, and Y. Gong, "Multiport driving topology for a photovoltaic aircraft light transmission system driven by switched reluctance motors," *Energies*, vol. 13, no. 14, p. 3687, Jul. 2020.
[32] C. Pica, R. Munteanu, S. Pavel, and H. Beleiu, "Modeling of photovoltaic panels," in *Proc. Int. Conf. Expo. Electr. Power Eng. (EPE)*, Iasi, Romania, Oct. 2018, pp. 769–773.

XIAOSHU ZAN (Member, IEEE) received the B.Eng. and Ph.D. degrees from the School of Information and Electrical Engineering, China University of Mining and Technology, Xuzhou, China, in 2003 and 2011, respectively. In 2001, he joined the School of Information and Electrical Engineering, China University of Mining and Technology, as a Lecturer. His research interests include switched reluctance motor, power electronics, and renewable power generation. He has published over ten articles in these areas.

GUANQUN XU was born in Jiangsu, China. He is currently pursuing the M.S. degree in electrical engineering with China University of Mining and Technology. His current research interests include operation and control of switched reluctance motors, current-sharing control, and novel power converters.

TIEJUN ZHAO was born in Sichuan, China. He is currently pursuing the M.S. degree in electrical engineering with China University of Mining and Technology. His current research interests include operation and control of switched reluctance generators, and the design of new switched reluctance motors.

RUIMING WANG received the M.S. degree in power system from North China Electric Power University, Beijing, China, in 2004. He is currently working with the China Electric Power Research Institute (State Key Laboratory of Operation and Control of Renewable Energy and Storage Systems). His special fields of research interests include wind power grid integration test technology and power system analysis.

LINWANG DAI received the M.S. degree in electrical engineering from Beijing Jiaotong University, Beijing, China, in 2014. He is currently with the China Electric Power Research Institute (State Key Laboratory of Operation and Control of Renewable Energy and Storage Systems). His research interests include renewable energy generation and grid-connected technology, power electronics, and electric drive.